

In preparation for ApJ, version of October 29, 2018

## Correlated timing and spectral behavior of 4U 1705–44

Jean-François Olive<sup>1</sup>, Didier Barret<sup>1</sup> & Marek Gierliński<sup>2,3</sup>

Olive@cesr.fr

### ABSTRACT

We follow the timing properties of the neutron star low-mass X-ray binary system 4U 1705–44 in different spectral states, as monitored by the Rossi X-ray Timing Explorer over about a month. We fit the power density spectra using multiple Lorentzians. We show that the characteristic frequencies of these Lorentzians, when properly identified, fit within the correlations previously reported. The time evolution of these frequencies and their relation with the parameters of the energy spectra reported in Barret & Olive (2002) are used to constrain the accretion geometry changes. The spectral data were fitted by the sum of a blackbody and a Comptonized component and were interpreted in the framework of a truncated accretion disk geometry, with a varying truncation radius. If one assumes that the characteristic frequencies of the Lorentzians are some measure of this truncation radius, as in most theoretical models, then the timing data presented here strengthen the above interpretation. The soft to hard and hard to soft transitions are clearly associated with the disk receding from and approaching the neutron star respectively. During the transitions, correlations are found between the Lorentzian frequencies and the flux and temperature of the blackbody, which is thus likely to be coming from the disk. On the other hand, in the hard state, the characteristic Lorentzians frequencies which are at the lowest, remained nearly constant despite significant evolution of the spectra parameters. The disk no longer contributes to the X-ray emission, and the blackbody is now likely to be emitted by the neutron star surface which is providing the seed photons for the Comptonization.

---

<sup>1</sup>Centre d'Etude Spatiale des Rayonnements, CNRS/UPS, 9 Avenue du Colonel Roche, 31028 Toulouse Cedex 04, France

<sup>2</sup>Department of Physics, University of Durham, South Road, Durham DH1 3LE, UK

<sup>3</sup>Uniwersytet Jagielloński, Obserwatorium Astronomiczne, ul. Orła 171, 30-244 Kraków, Poland

*Subject headings:* X-rays: star, stars: individual: 4U 1705–44, stars: neutron, accretion, accretion disks

## 1. Introduction

Rapid X-ray variability is a powerful probe of physics of accretion flows around neutron stars and black holes. Significant progress has been accomplished recently with the advent of the *Rossi X-ray Timing Explorer* (*RXTE*, Bradt, Rothschild & Swank 1993). Its large collecting area and micro-second time resolution allowed us to study with exquisite details the rapid variability of a wide variety of accreting X-ray sources. In particular, the power density spectra (PDS) of Galactic black hole candidates and neutron star low-mass X-ray binaries (LMXBs) exhibit a variety of features ranging from narrow quasi-periodic oscillations (QPOs) to broad noise components (for a review see Wijnands 2001 and references therein).

It has been shown recently that these PDS can be well represented as a superposition of a few Lorentzians (e.g. Olive et al. 1998; Van Straaten et al. 2002; Belloni, Psaltis & Van der Klis 2002). The multi-Lorentzian approach gives a simple and universal phenomenological description of the PDS. Each noise component (Lorentzian) is then described by its characteristic frequency, width and amplitude, usually expressed as a fractional root-mean-square (RMS). It has been demonstrated that these characteristic frequencies are correlated for a given source and between sources, both for neutron star and black hole binaries (Wijnands & Van der Klis 1999; Psaltis, Belloni & van der Klis 1999; Belloni et al. 2002). In most models of rapid X-ray variability, these frequencies are related to some kind of an abrupt transition in the accretion disk (e.g. Stella, Vietri & Morsink 1999; Titarchuk & Osherovitch 1999; Psaltis & Norman 2002). This could be a truncation of a Shakura-Sunyaev disk into a hot inner flow (e.g. Różańska & Czerny 2000). With the truncation radius decreasing (the disk coming in) the characteristic frequencies increase.

4U 1705–44 is a neutron star LMXB system which belongs to the class of atoll sources (Hasinger & Van der Klis 1989). The source shows variability on all time scales, from months down to milliseconds (Langmeier et al. 1987; Berger & Van der Klis 1998, Ford, van der Klis & Kaaret 1998, Liu, van Paradijs & van den Heuvel 2001 and references therein). On long time scales, it displays clear luminosity-related spectral changes. This is illustrated in the observations reported by Barret & Olive (2002; hereafter Paper I) who followed the spectral evolution of the source during a transition between soft and hard X-ray spectral states. The data were interpreted in the framework of a truncated accretion disk geometry for which the spectral transitions observed were associated with changes in the disk truncation radius.

In this paper, we follow the multi-Lorentzian approach to study the rapid X-ray variability of the source using the same set of observations as presented in Paper I. The aim of this work is to look for correlations between the timing and spectral parameters to get further insights on the accretion flow changes associated with the state transitions.

## 2. Observation and data analysis

We use the same set of *RXTE* observations as in Paper I. The data cover a period from February 10th to March 9th, 1999, with pointings performed every two days, giving 14 observations in total. In the following the observations are numbered from 1 to 14. During this period, the source X-ray count rate first decreased, reached a minimum around observation 6, and then increased to reach the initial level (see top of Fig. 1). On the X-ray color-color diagram (bottom of Fig. 1), the source traced out part of a more or less triangular pattern (see also Gierliński & Done 2002). 4U 1705–44 evolved from the soft (the so-called banana) to the hard (island) state in  $\sim 10$  days, remained in a hard state for  $\sim 12$  days, and then moved back to the soft state in  $\sim 4$  days. In Paper I, all fourteen energy spectra were adequately fitted by the sum of a blackbody, thermal Comptonization and an iron line.

For timing analysis we use the science event data obtained in configuration E\_16us\_64M\_0\_1s. We have computed 0.03–4096 Hz PDS in the 3–30 keV energy range, for the same time intervals as the energy spectra. The Poisson counting noise level was estimated from the data above 1500 Hz and subtracted from the PDS before fitting. Each PDS has been rebinned using a logarithmic scheme, and expressed in terms of fractional RMS amplitude.

We have fitted each of the 14 PDS by up to 4 Lorentzians with the following analytical formula given below (van Straaten et al. 2002):

$$P_\nu = \frac{r^2 \Delta}{\left(\frac{\pi}{2} + \arctan 2Q\right) [\Delta^2 + (\nu - 2\Delta Q)^2]}, \quad (1)$$

where  $\Delta \equiv \nu_{\max} / \sqrt{1 + 4Q^2}$  is the half width at half maximum of the Lorentzian and  $\nu_{\max}$  (the position of the maximum of the Lorentzian per logarithmic frequency interval, i.e. the peak position of  $\nu P_\nu$ ),  $r$  (the fractional RMS integrated from 0 to  $\infty$ ) and  $Q$  (the quality factor) are the independent parameters to fit. The centroid of the Lorentzian ( $\nu_0$ ) is related to the above parameters as:  $\nu_0 \equiv 2\Delta Q = \sqrt{\nu_{\max}^2 - \Delta^2}$ . The spectral fitting and error computations were carried out using XSPEC 11.1 (Arnaud et al. 1996). Whenever the  $Q$  parameter was consistent with zero, we used zero-centered Lorentzians ( $Q$  frozen at 0). Finally, we searched for kHz QPOs using the PDS scanning technique described in Boirin et al. (2000).

### 3. Results

The spectra together with the best-fitting models are presented in Fig. 2. The best fit parameters are listed in Tab. 1. Time evolution of the fitted Lorentzian frequencies is shown in Fig. 3. In those observations with the best statistics (7 to 13), three broad components are detected with noise extending up to  $\geq 500$  Hz. kHz QPOs around 750–800 Hz were detected above the  $3\sigma$  level in observations 1, 2 and 14 (see Tab. 2) when the source was in the soft state. Our frequencies are close to those reported by Ford et al. (1998) using observations performed in February to June 1997 while the source was in a similar spectral state. In terms of fractional RMS, the sensitivity to QPO detection decreases with the source count rate. For indication,  $3\sigma$  upper limits of 4.6, 8.5, 6.2, 5.0, 4.5, 3.4% can be derived for a QPO at 750 Hz with a 20Hz width in observations 3, 5, 7, 9, 11, 13 respectively. However, in terms of modulated amplitude, the signals detected in observations 1, 2 and 14 would have been clearly detected in the other observations.

Narrow QPOs around  $\sim 170$  Hz were found in observations 2 and 3 ( $\nu = 162_{-7}^{+3}$  Hz,  $\text{RMS}(\%) = 2.9 \pm 0.7$  for observation 2 and  $\nu = 178_{-10}^{+10}$  Hz,  $\text{RMS}(\%) = 4.5 \pm 1.0$  for observation 3). Similar QPOs, called hecto-Hz QPOs have been reported from other sources (e.g. van Straaten et al. 2002). The PDS of observation 2 is also remarkable by the presence of a very low frequency component (VLFN, see Fig. 2), not seen in other observations. A fit with a zero-centered Lorentzian of this component yields  $\nu_{\text{max}} = 0.156_{-0.04}^{+0.06}$  Hz and  $\text{RMS}(\%) = 3.1 \pm 0.4$ . These transient features will not be discussed in this paper.

#### 3.1. Identification of the PDS components

The PDS of 4U 1705–44 resemble those reported by Belloni et al. (2002) and van Straaten et al. (2002) from similar systems. Following Belloni et al. (2002), we name the first two Lorentzians as band limited noise (BLN at  $\nu_b \sim 1\text{--}7$  Hz) and low-frequency noise (LFN at  $\nu_{\text{LF}} \sim 7\text{--}40$  Hz). The LFN component is the only one which can be identified in all observations. In Fig. 4, we plot  $\nu_{\text{LF}}$  versus  $\nu_b$ . A clear correlation can be seen. Our results can be directly compared with those obtained for some other neutron star LMXBs. Taking out the same two components in Belloni et al. (2002) for 1E 1724-3045 and GS 1826-34 and van Straaten et al. (2002) for 4U 1728-34 and 4U 0614+091 (in the latter paper  $\nu_b$  is called  $\nu_{\text{BLN}}$ ), we find that our data points fall in on the global correlation previously reported by these authors. This supports the identification of the first two components of the PDS of 4U 1705–44 with BLN and LFN.

The third broad Lorentzian component which we denote as high frequency noise (HFN

at characteristic frequencies of  $\sim 60\text{--}400$  Hz) is detected only in data sets 7 to 13. It is the one which is the less statistically significant, and its identification is therefore less certain. It may be the hecto-Hz component reported by van Straaten et al. (2002) from similar systems. However, these hecto-Hz components are generally narrower than the features we observed in 4U 1705–44 which are fitted with zero-centered Lorentzians. It seems therefore more likely to be what is called  $L_l$  in Belloni et al. (2002); namely the extrapolation towards low frequencies of the lower kHz QPO. Support from that hypothesis comes from the fact our data points match the global correlation between  $\nu_{\text{LF}}$  and  $\nu_l$  discovered by Psaltis et al. (1999). This feature would then be closely related to the lower kHz QPOs detected in observations 1, 2 and 14. As expected, the kHz QPO frequencies fit in the global correlation (see Fig. 5).

### 3.2. Correlation between PDS and energy spectrum parameters

Since the LFN component is detected in all observations and since the other frequencies are correlated with  $\nu_{\text{LF}}$ , we used  $\nu_{\text{LF}}$  for searching correlations between PDS and energy spectrum parameters.

We split the observation in 3 segments: the transition the soft to hard state (T1, obs. 1 to 6), the observations corresponding to the island state (IS, obs. 6 to 12), the transition hard to soft (T2, obs. 12 to 14). In Fig. 6, 7 and 8, we plot  $\nu_{\text{LF}}$  versus the soft and hard colors,  $\nu_{\text{LF}}$  versus the blackbody temperature and bolometric flux and  $\nu_{\text{LF}}$  versus the electron temperature of the Comptonizing cloud ( $kT_e$ ) and 20–200 keV hard X-ray flux ( $F_{\text{Hard}}$ ).

Fig. 6 shows that there is a clear anti-correlation between  $\nu_{\text{LF}}$  and HR2 in all three segments. On the other hand, there are no obvious correlations between  $\nu_{\text{LF}}$  and HR1. This is consistent with previous work which have shown that timing features, such as kHz QPOs (whose frequencies correlate with  $\nu_{\text{LF}}$ , see above) anti-correlate with the hard color (e.g. Méndez et al. 1999).

Fig. 7 clearly shows a nice correlation between  $\nu_{\text{LF}}$  and the blackbody temperature and flux at the start of the soft to hard transition (obs. 1 to 3) and during the reverse transition (obs. 12 to 14). Similar correlations between the blackbody flux and kilo-QPO frequencies have been already reported from 4U 0614+091 (Ford et al. 1997). Here we show that the correlations break down in 4U 1705–44 when the blackbody flux dropped below  $\sim 10^{-10}$  ergs  $\text{s}^{-1} \text{cm}^{-2}$ . Down in the IS, the absence of correlation is striking, despite the smooth but significant increase of the blackbody flux and temperature.

Finally, Fig. 8 shows that during T1 and T2 there is a clear anti-correlation between

$\nu_{\text{LF}}$  and both  $kT_e$  and  $F_{\text{Hard}}$ , and there are no obvious correlations of these two parameters with  $\nu_{\text{LF}}$  in IS (no correlations with time are present either).

#### 4. Discussion

In most of the rapid variability models the frequencies of particular noise components are set at some transition radius in the disk (e.g. Stella et al. 1999; Psaltis & Norman 2002). It could be for instance a truncation of a standard Shakura-Sunyaev disk into a hot inner flow. Here we assume that the frequencies we observe, in particular  $\nu_{\text{LF}}$  which can be traced throughout all the data sets, are related to the truncation radius of the disk. In Paper I we interpreted the spectral state transitions in the framework of a such truncated accretion disk geometry, allowing the truncation radius to change within the observations. Let us now discuss the new constraints that the data presented above set on this scenario.

At the beginning of our observations (obs. 1–2), the source is in the soft state, the truncation radius is small and the disk is close to the neutron star surface (see Paper I). The characteristic frequency  $\nu_{\text{LF}}$  is at its maximum around 40 Hz, which is consistent with the inner disc radius reaching its minimum. It is also the time during which the kHz QPOs at 750–780 Hz are detected. If the latter one is associated with the Keplerian frequency at the truncation radius, the disk truncates at  $\sim 20$  km. The soft component ( $kT_{\text{BB}} \sim 1.8$  keV) present in the energy spectrum originates from the disk (Paper 1). The hard component is from the boundary layer, with low temperature of  $kT_e \sim 4$  keV.

In Paper I, we suggested that during the transition to the hard state (T1, obs. 2 to 6) the disk receded while the total source luminosity decreased from  $\sim 2.1$  to  $0.7 \times 10^{37}$  ergs  $\text{s}^{-1}$ . This is supported by our timing analysis: during the transition  $\nu_{\text{LF}}$  dropped roughly by factor of  $\sim 6$ . The fastest variability timescale around a compact object is given by the Keplerian orbital frequency (at  $\nu_k$ ). This sets an upper bound on the inner radius of the disk at which the variability is produced (see e.g. di Matteo & Psaltis 1999). When  $\nu_k$  is not detected, one can use the empirical correlation found by Psaltis et al. (1999) between  $\nu_k$  and  $\nu_{\text{LF}}$  to estimate the inner disk radius as a function of  $\nu_{\text{LF}}$  (see equation 2 in di Matteo & Psaltis 1999). Using the latter equation, one obtains a disk truncation radius around 70 km for observation 6. When the disk recedes, the temperature and flux of the soft component drop to their lowest values ( $kT_{\text{BB}} \sim 0.8$  keV, Fig. 7, left panels). Meanwhile, the hot inner flow (or optically thin boundary layer) builds up and its temperature rises from  $\sim 4$  to  $\sim 14$  keV (Fig. 8, left panels) possibly because the disk contribution to the cooling of the inner flow is then seriously reduced.

Between observations 6 and 12 (IS) the source is in the hard state while the mass accretion rate (inferred from the source luminosity  $L_{0.1-200} \sim 0.7$  to  $2.5 \times 10^{37}$  ergs  $s^{-1}$ ) monotonically increased. The energy spectrum is dominated by the emission from the hot optically thin inner flow (Paper I). In the proposed scenario, the disk is far away, and  $\nu_{LF}$  is low,  $\sim 7-12$  Hz. With the exception of observation 6, all the PDS show three broad Lorentzians (at  $\nu_b$ ,  $\nu_{LF}$  and  $\nu_l$ ) at characteristic frequencies which are roughly constant suggesting that the geometry of accretion remains similar through these observations. There is no correlation between  $\nu_{LF}$  (which is roughly stable) and the blackbody flux and temperature either (Fig. 7, right panels) despite significant variations of these parameters. During this hard state, the spectral and the timing parameters are *de-correlated*. This can be naturally explained if the soft component (blackbody) originates from the neutron star surface, not from the disk. Basically, the disk is far away and its temperature is so low that it cannot be seen by the PCA, so it does not contribute to the energy spectrum. We can see its variations only through the timing properties, as  $\nu_{LF}$ . The blackbody comes from the neutron star surface which is continuously heated along these observations. This soft component is further Comptonized in the optically thin hot inner flow/boundary layer leading to an increasing  $F_{20-200}$  flux (Fig. 8, right panel). It is also important to note that at the end of the IS state (obs. 12), the source has recovered an accretion rate (as inferred with the luminosity) similar to observations 1 or 2, while the truncation radius of the disk (as traced with  $\nu_{LF}$ ) is still large.

The transition back to the soft state (T2, obs. 12 to 14) is the inverse of the T1 transition. The blackbody flux and temperature increased, which was interpreted (Paper I) as the reappearance in the PCA energy band of the disc moving in and becoming hotter. Again, the timing analysis supports this result: there is a significant increase in  $\nu_{LF}$ , very well correlated both with  $T_{bb}$  and  $F_{bb}$ . Meanwhile, the inner flow is significantly cooled by the increasing flux of soft photons coming from the disk and its temperature falls from  $\sim 10$  to  $\sim 4$  keV. In observation 14, the system is back to a state very similar to observation 1 and 2, and we start seeing again kHz QPO at  $\sim 750$  Hz.

It is also interesting to look at rapid X-ray variability as a function of the position in the color-color diagram. Both atolls and Z sources trace out a characteristic track in the diagram (see e.g. Hasinger & van der Klis 1989). The frequencies in the PDS are usually very well correlated with the position in the diagram. It has been shown recently that at low luminosities atolls form an additional, upper horizontal branch in the color-color diagram, tracing out a Z-shaped track, similar to Z sources (Gierliński & Done 2002; Munro, Remillard & Chakrabarty 2002).

4U 1705–44 moved from left to right in the horizontal branch between observations 6 and

12, and then along the diagonal, between observations 12 and 14 (Fig. 1). The timing and spectral properties on the diagonal branch are typical of other atoll sources. However, the upper branch is different: as we discussed previously, there is no correlation between  $\nu_{\text{LF}}$  and the position on the branch, which in this case (branch is horizontal) can be described by the soft color HR1 (see Fig. 6).

In our scenario, at low accretion rate, the position in the upper branch of the diagram is set by the neutron star temperature, which also supplies the seed photons. With the increasing accretion rate,  $\dot{M}$ , this temperature increases, so does the temperature of the low-energy cutoff in the Comptonized component. The spectrum below 4 keV hardens, so the soft color increases and the source moves to the right in the diagram. This movement is *not* accompanied by the decrease of the truncation radius in the disk. Then, on the diagonal branch the disk temperature increases, so it can be seen in the PCA spectrum, while the neutron star surface is obscured by the increasing optical depth of the boundary layer. Thus, both spectral and timing properties depend now on the disk, and therefore are correlated. In this picture, the position on the upper branch depends on  $\dot{M}$ , while the characteristic frequency  $\nu_{\text{LF}}$  do not.

The path of 4U 1705–44 in the color-color diagram is even more complicated. On its way from the banana to the island state (T1) it traces out a different track than in the opposite direction (T2). The timing and spectral properties on both tracks are different. For instance observations 3 and 13 have very similar  $\nu_{\text{LF}}$ , but different bolometric luminosities ( $L_{0.1-200} = 1.4 \times 10^{37} \text{ergs s}^{-1}$ ,  $2.4 \times 10^{37} \text{ergs s}^{-1}$  respectively, see Paper I) and different power density spectra (see Fig. 2). This shows that for the same truncation radius, one can have different instantaneous accretion rate as derived from the source luminosity, and different time variability (the Lorentzians at  $\nu_b$  and  $\nu_l$  are not detected in observation 3). In the proposed scenario, there are however important differences between observations 3 and 13 (and more generally between T1 and T2). In the first case, the disk recedes, the luminosity is decreasing, whereas in obs. 13 the disk approaches the neutron star and the luminosity is increasing. This means that the state of the system depends at some level on its recent history. Any models proposed to explain the changes in  $\nu_{\text{LF}}$  must take this fact into account.

One possibility could be that  $\nu_{\text{LF}}$  (i.e the truncation radius) is set by some long-time averaging process over time scales of days and only depends on a parameter  $\eta = \dot{M}_d / \langle \dot{M}_d \rangle$  (where  $\dot{M}_d$  is the accretion rate through the disk) similarly to what has been proposed by van der Klis (2001) to explain the parallel tracks phenomenon in LMXBs. This model naturally predicts the decorrelation between the truncation radius position and the total accretion rate (and so the luminosity). In that scheme, the motion of the disk is associated with a rapid decrease of  $\dot{M}_d$  during the T1 transition (i.e  $\eta < 1$ , decreasing with time, the disk recedes)



and a reversed evolution during T2. The disk is stable either if  $\dot{M}_d$  is constant or if it varies linearly with time over several days. This could be the case from observations 6 to 12 when  $\nu_{\text{LF}}$  was low and roughly stable.

## 5. Conclusions

The spectral and timing data of the state transitions observed from 4U 1705–44 can be explained in the framework of a model, in which the critical parameter is the position of the truncation radius between the disk and a hotter inner flow. This parameter sets both the frequencies of the timing features and the spectral shape. What sets the value of the truncation radius is unclear at the moment, but both the timing and spectral data indicate that it cannot be the mass accretion rate derived from the bolometric source luminosity. One possibility could be this radius is set by some long-time averaging process over time scales of days.

## REFERENCES

- Arnaud, K.A., 1996, *Astronomical Data Analysis Software and Systems V*, eds. Jacoby G. and Barnes J., p17, ASP Conf. Series volume 101.
- Barret, D. & Olive, J.F., 2002, *ApJ*, in press, astro-ph/0205184
- Boirin, L., Barret, D., Olive, J. F., Bloser, P. F., & Grindlay, J. E. 2000, *A&A*, 361, 121
- Bradt, H., Rothschild, R., E., Swank, J. H., 1993, *A&AS*, 97, 355
- Belloni, T., Psaltis, D., & van der Klis, M. 2002, *ApJ*, 572, 392
- Berger, M. & van der Klis, M. 1998, *A&A*, 340, 143
- Gierliński, M. & Done, C. 2002, *MNRAS*, 331, L47
- Ford, E. C. et al. 1997, *ApJ*, 486, L47
- Ford, E. C., van der Klis, M., & Kaaret, P. 1998, *ApJ*, 498, L41
- Hasinger & van der Klis, 1989, *A&A*, 225, 79
- Langmeier, A., Sztajno, M., Hasinger, G., Truemper, J., & Gottwald, M. 1987, *ApJ*, 323, 288
- Liu, Q. Z., van Paradijs, J., & van den Heuvel, E. P. J. 2001, *A&A*, 368, 1021
- Méndez, M, van der Klis, M, Ford, E., Wijnands, R., van Paradijs, J. 1989, *ApJ*, 511, L49
- di Matteo, T. & Psaltis, D. 1999, *ApJ*, 526, L101
- Muno, M. P., Remillard, R. A., & Chakrabarty, D. 2002, *ApJ*, 568, L35
- Olive, J. F., Barret, D., Boirin, L., Grindlay, J. E., Swank, J. H., & Smale, A. P. 1998, *A&A*, 333, 942
- Psaltis, D., Belloni, T., & van der Klis, M. 1999, *ApJ*, 520, 262
- Psaltis, D. & Norman C., 2002, *ApJ*, submitted, astro-ph/0001391
- Stella, L., Vietri, M., & Morsink, S. M. 1999, *ApJ*, 524, L63
- Rózańska, A. & Czerny, B. 2000, *MNRAS*, 316, 473
- Titarchuk, L. & Osherovich, V. 1999, *ApJ*, 518, L95

van der Klis, M. 2001, ApJ, 561, 943.

van Straaten, S., van der Klis M., di Salvo T., Belloni T. & Psaltis D., 2002, ApJ, in press,  
astro-ph/0107562

Wijnands, R. 2001, Advances in Space Research, 28, 469

Wijnands, R. & van der Klis, M., 1999, ApJ, 514, 939

### 6. Tables

Obs	$\nu_b$	RMS <sub>b</sub>	$\nu_{LF}$	RMS <sub>LF</sub>	$Q_{LF}$	$\nu_l$	RMS <sub>l</sub>	$\chi^2/d.o.f$
01	...	...	$37.11^{+12.5}_{-9.7}$	$5.9^{+0.6}_{-0.6}$	(0)	...	...	101.3/93
02	...	...	$45.03^{+7.0}_{-5.0}$	$4.9^{+0.9}_{-0.9}$	$0.91^{+0.8}_{-0.5}$	...	...	77.3/89
03	...	...	$25.13^{+2.5}_{-2.2}$	$12.7^{+0.4}_{-0.5}$	(0)	...	...	96.8/94
04	$5.63^{+1.5}_{-1.3}$	$7.8^{+1.0}_{-1.4}$	$23.32^{+5.4}_{-3.7}$	$7.3^{+3.0}_{-1.8}$	$0.56^{+0.5}_{-0.4}$	...	...	105.8/87
05	$0.87^{+2.0}_{-0.5}$	$4.6^{+0.4}_{-0.4}$	$9.46^{+3.9}_{-1.8}$	$8.7^{+0.8}_{-2.2}$	(0)	...	...	102.1/93
06	$0.83^{+0.2}_{-0.2}$	$7.7^{+0.2}_{-0.3}$	$7.18^{+2.0}_{-0.8}$	$8.9^{+3.5}_{-0.6}$	$0.36^{+0.1}_{-0.4}$	...	...	98.2/93
07	$1.51^{+0.2}_{-0.1}$	$8.9^{+0.4}_{-0.4}$	$11.72^{+1.0}_{-0.9}$	$9.3^{+1.1}_{-1.1}$	$0.67^{+0.2}_{-0.2}$	$363^{+667}_{-221}$	$11.3^{+2.8}_{-2.8}$	98.1/91
08	$1.49^{+0.1}_{-0.2}$	$8.0^{+0.3}_{-0.4}$	$9.91^{+0.7}_{-0.7}$	$8.2^{+1.0}_{-0.8}$	$0.67^{+0.2}_{-0.2}$	$254^{+165}_{-126}$	$9.8^{+1.5}_{-1.6}$	102.3/91
09	$0.95^{+0.1}_{-0.1}$	$10.0^{+0.2}_{-0.2}$	$6.42^{+0.3}_{-0.3}$	$11.1^{+0.9}_{-0.5}$	$0.55^{+0.1}_{-0.1}$	$86^{+40}_{-29}$	$10.6^{+8.1}_{-0.8}$	127.6/91
10	$1.29^{+0.1}_{-0.1}$	$10.8^{+0.3}_{-0.4}$	$7.63^{+0.5}_{-0.6}$	$10.3^{+1.6}_{-1.9}$	$0.69^{+0.3}_{-0.2}$	$58^{+69}_{-31}$	$9.9^{+0.7}_{-0.7}$	127.0/91
11	$1.47^{+0.1}_{-0.2}$	$8.7^{+0.4}_{-0.4}$	$7.67^{+0.4}_{-0.4}$	$9.1^{+1.1}_{-1.1}$	$0.65^{+0.2}_{-0.1}$	$56^{+39}_{-21}$	$8.4^{+0.6}_{-0.7}$	112.9/91
12	$1.78^{+0.1}_{-0.2}$	$10.7^{+0.2}_{-0.4}$	$10.33^{+0.3}_{-0.3}$	$11.2^{+0.7}_{-0.5}$	$0.65^{+0.1}_{-0.1}$	$147^{+42}_{-33}$	$10.0^{+0.7}_{-0.7}$	149.0/91
13	$6.29^{+0.6}_{-0.6}$	$10.0^{+0.4}_{-0.5}$	$27.43^{+1.5}_{-1.5}$	$8.8^{+0.9}_{-0.9}$	$0.69^{+0.2}_{-0.1}$	$338^{+254}_{-141}$	$7.8^{+1.1}_{-0.6}$	100.3/91
14	...	...	$37.93^{+6.0}_{-5.2}$	$7.6^{+0.4}_{-0.4}$	(0)	...	...	104.6/93

Table 1: Best fit parameters for the 14 PDS.  $\nu_b$  and RMS<sub>b</sub> are respectively the frequency and the RMS of the band-limited noise component fitted with a zero-centered lorentzian.  $\nu_{LF}$  RMS<sub>LF</sub> and  $Q_{LF}$  are the frequency, the RMS and the Quality factor of the Low-Frequency Noise component detected in all observations.  $\nu_l$  and RMS<sub>l</sub> are the frequency and RMS of the high frequency noise component. The naming convention follows Belloni et al. (2002). Finally,  $\chi^2/d.o.f$  is the  $\chi^2$  value and the number of degree of freedom of the fit.

Obs	$\nu$ (Hz)	RMS (%)	Q
01	$751^{+6}_{-5}$	$3.5^{+1.2}_{-0.8}$	$31^{+33}_{-13}$
02	$783^{+8}_{-7}$	$2.9^{+1.1}_{-1.0}$	$41^{+40}_{-24}$
14	$748^{+26}_{-47}$	$3.8^{+1.0}_{-1.0}$	(10)

Table 2: The best fit parameters (frequency, RMS and the quality factor Q) for the kHz QPOs detected in observations 1, 2 and 14. For observation 14, the Q value was poorly constrained and then frozen at 10 for the fit. These frequencies are consistent with those reported by Ford et al. (1998).

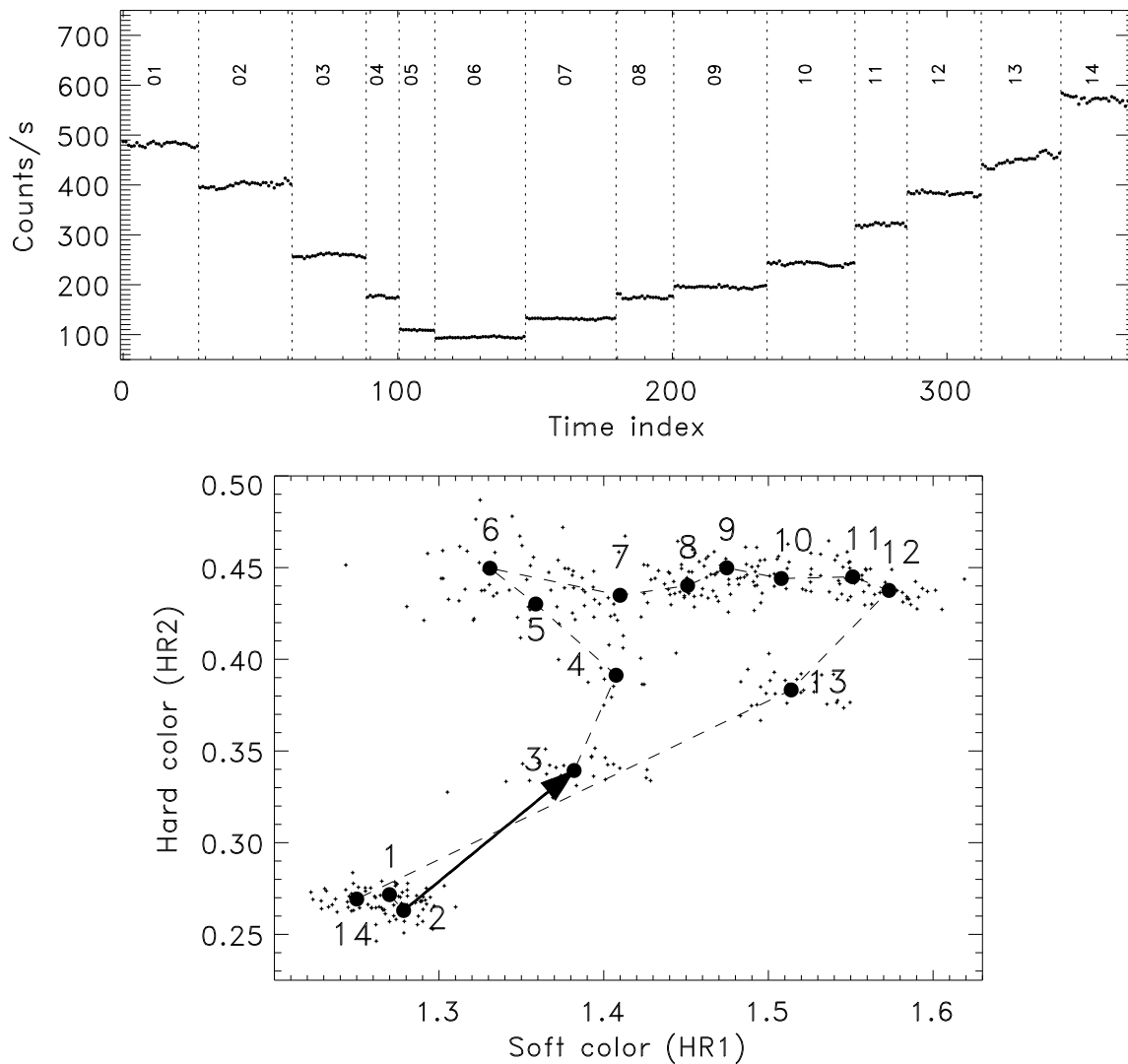


Fig. 1.— The PCA background subtracted light curve of the 4U 1705–44 in the 3–16 keV band (top panel). The data are plotted versus a time index to avoid the gaps in time between observations. The bottom panel shows the X-ray color-color diagram of 4U 1705–44. The soft color (HR1) is defined as the ratio between the 4.3–6.5 keV counts and 2.9–4.3 keV counts, and the hard color (HR2) as the ratio between the 10.1–16.2 keV counts and 6.5–10.1 keV counts. The observation numbers allow to follow the path of the source during the state transitions.

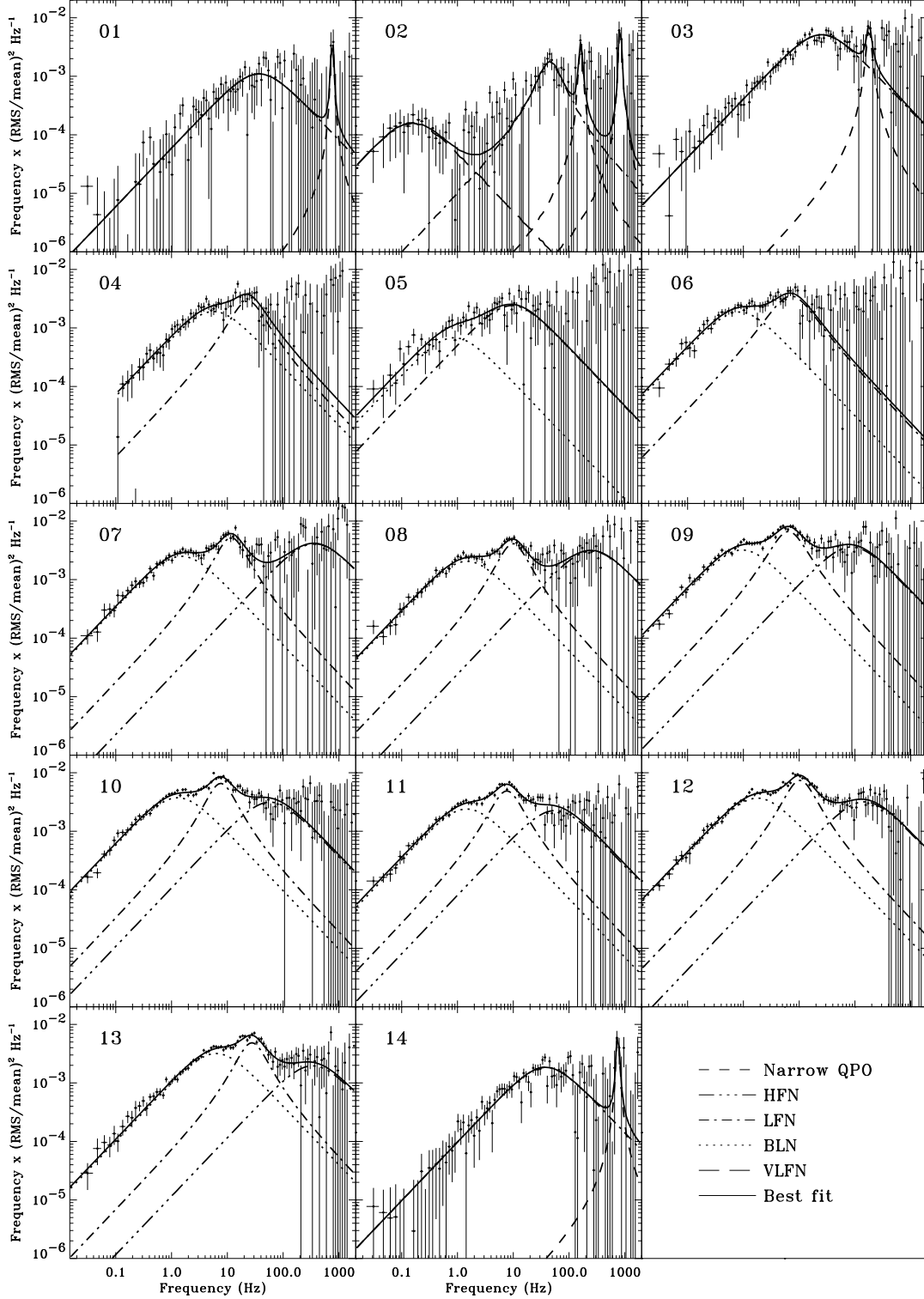


Fig. 2.— The 14 power density spectra (PDS) from 4U 1705–44 fitted by up to four Lorentzians. HFN stands for High Frequency Noise, LFN for Low-Frequency Noise, BLN for Band-Limited Noise and VLFN for Very-Low Frequency Noise. Narrow Quasi-Periodic Oscillations (QPOs) were also detected in observations 1, 2, 3 and 14.

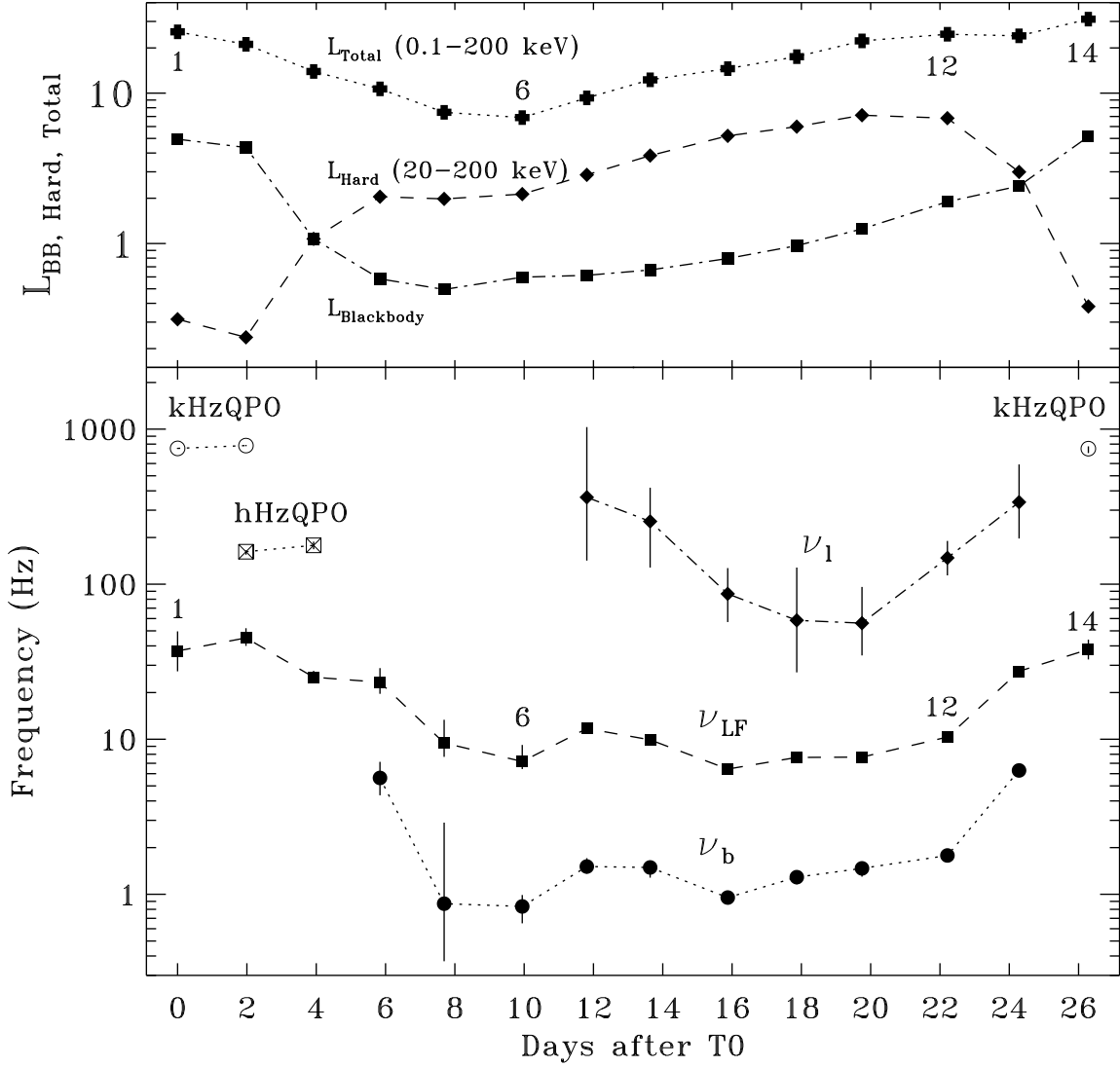


Fig. 3.— Top panel: The luminosities ( $L_{\text{Total}}$ ,  $L_{\text{Hard}}$  and  $L_{\text{Blackbody}}$ ) along the 14 observations in units of  $10^{36} \text{ ergs s}^{-1}$ . Bottom panel: Time evolution of the PDS fitted parameters.  $\nu_b$  is the frequency of the lorentzian fitting the BLN component of Fig. 2,  $\nu_{\text{LF}}$  is the frequency of the LF lorentzian,  $\nu_1$  is the HFN Lorentzian. The naming convention follows Belloni et al. (2002). Hecto-Hz QPOs were detected in observations 2 and 3. kHz QPOs were detected in observations 1, 2 and 14. As can be seen  $\nu_{\text{LF}}$  is the only component which is detected in all observations.

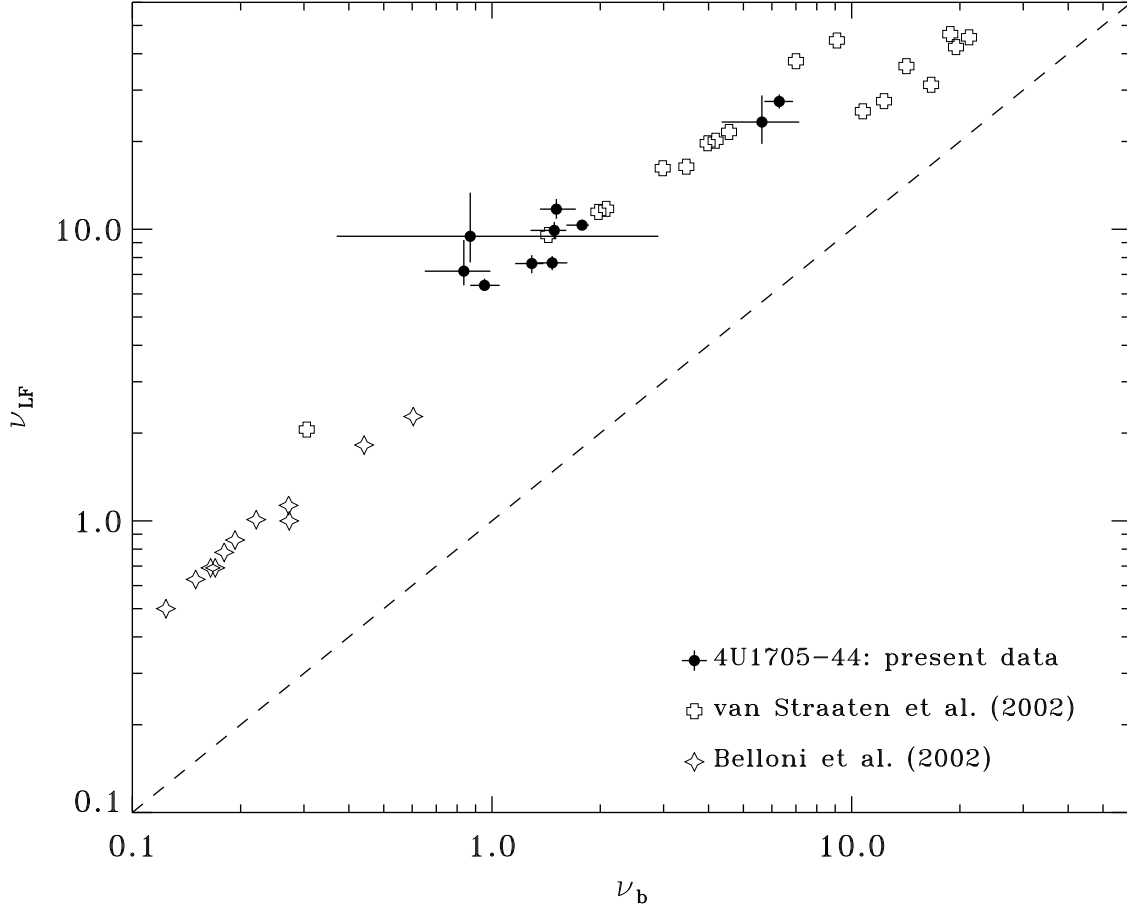


Fig. 4.—  $\nu_{LF}$  as a function of  $\nu_b$ . Data points from 4U 1705–44 are plotted with a filled circle. They are compared with those obtained for systems similar to 4U 1705–44 for which the same type of multi-lorentzian fitting of the PDS was performed (Empty stars : GS 1826–34, 1E 1724–3045 and SLX 1735–369; Belloni et al. (2002). Empty crosses : 4U 0614+091 and 4U 1728–34; van Straaten et al. (2002)) Our data point fit in the correlation, indicating that the identification of the various frequencies of the PDS is correct.



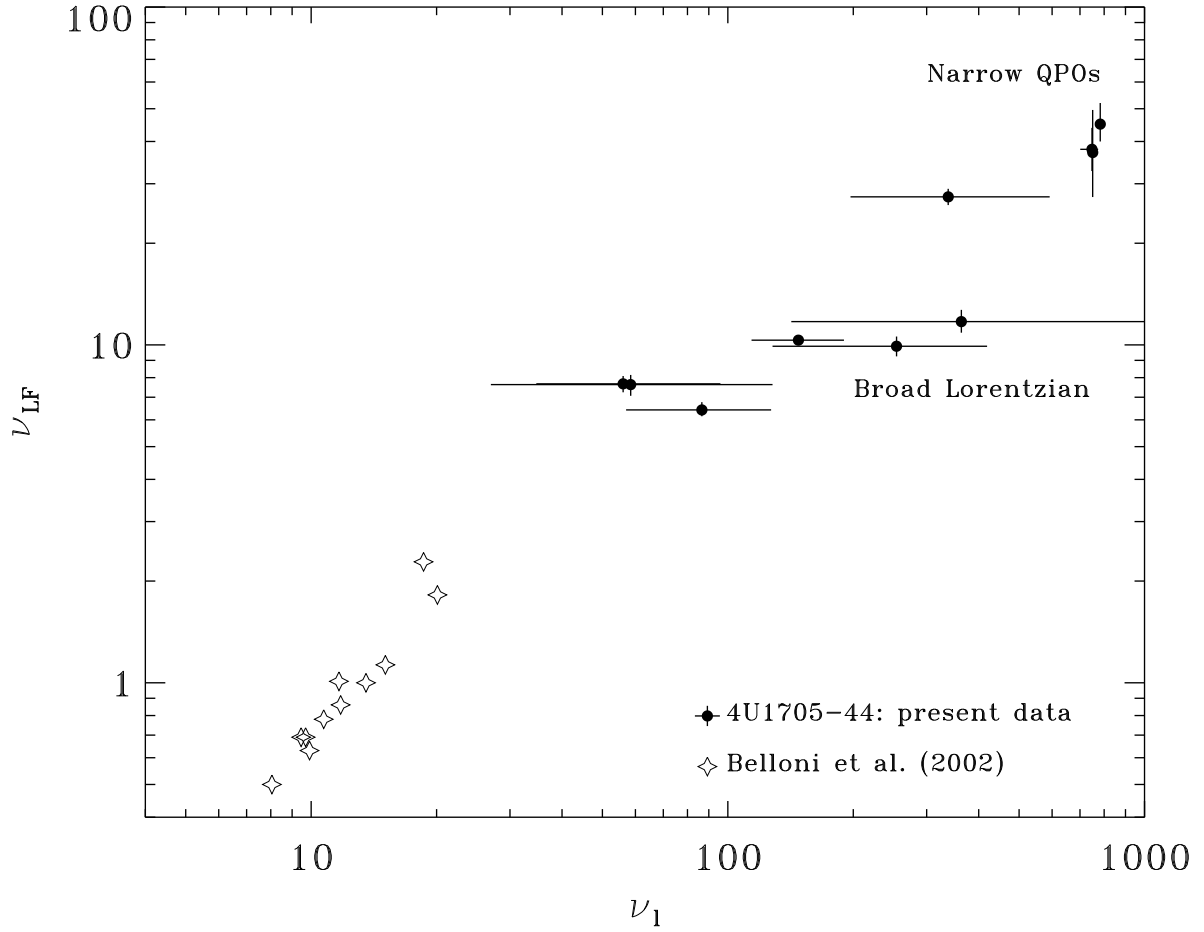


Fig. 5.—  $\nu_{LF}$  as a function of  $\nu_l$ . For comparison data points from Belloni et al. (2002) are also shown. Again, a correlation has been shown to exist in many systems (Psaltis et al. 1999; Belloni et al. 2002).  $\nu_l$  and the three kHz QPO frequencies follow the correlation.

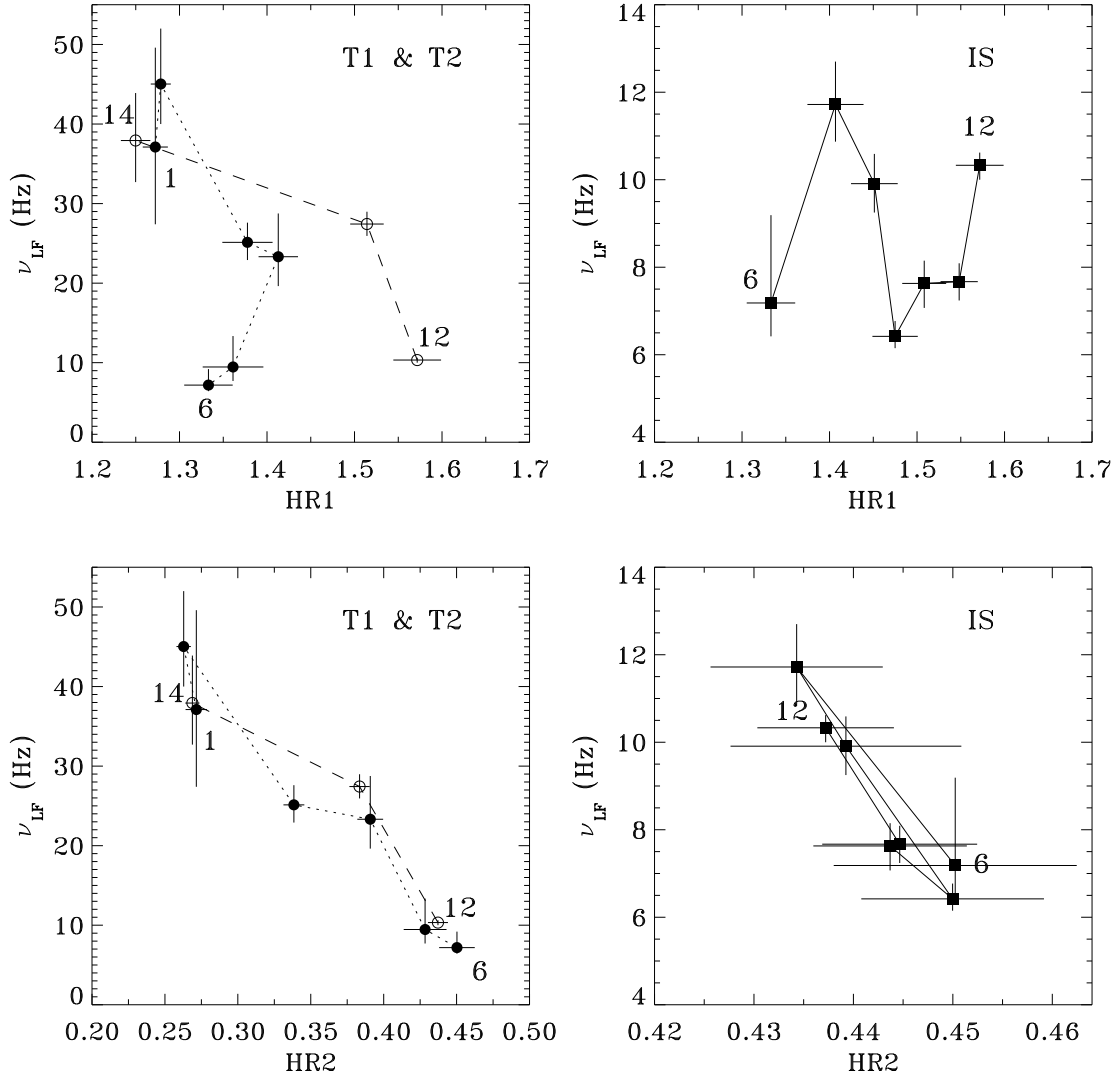


Fig. 6.—  $\nu_{LF}$  as a function of HR1 and HR2. Three segments of the observations are considered: T1 is the transition which occurred between observations 1 and 6 (filled circles), IS is the Island State between observations 6 and 12 (empty squares) and T2 is the transition between observations 12 and 14 (empty circles).

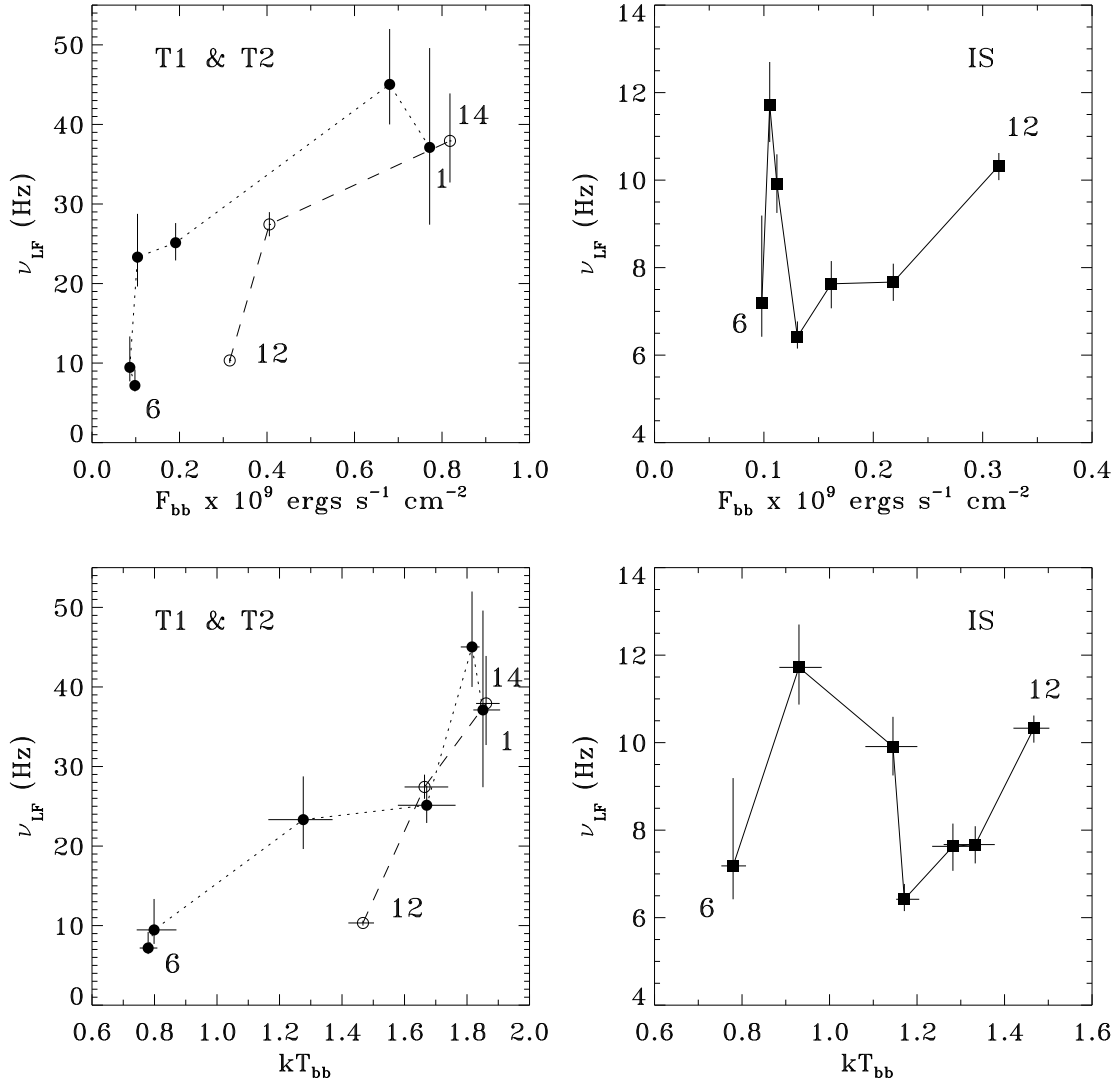


Fig. 7.—  $\nu_{LF}$  as a function of the blackbody temperature and flux for the three segments of observations.

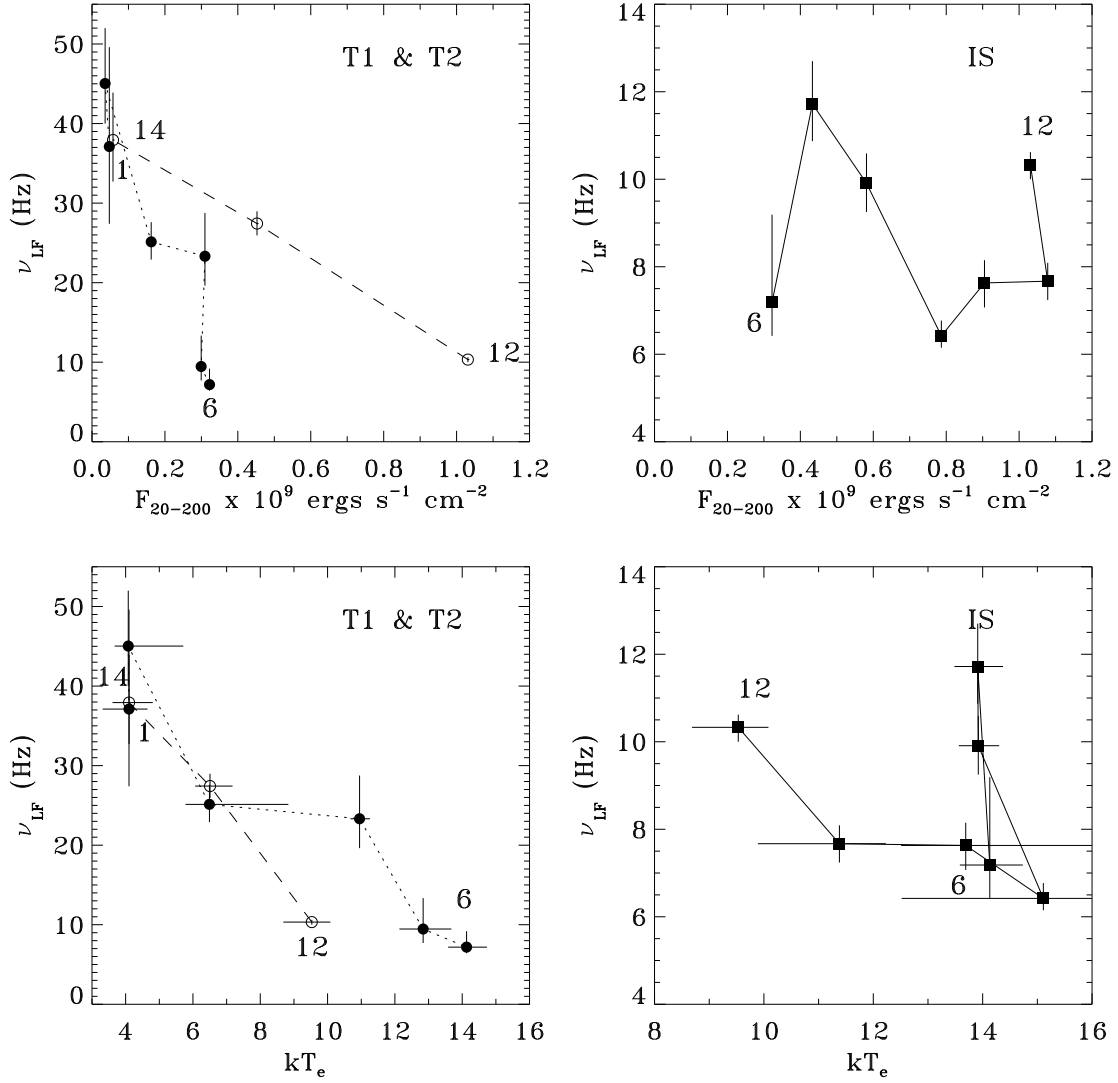


Fig. 8.—  $\nu_{LF}$  as a function of the electron temperature and the bolometric flux between 20 and 200 keV for the three segments of observations.